Nickel Block of Three Cloned T-Type Calcium Channels: Low Concentrations Selectively Block α1H

Jung-Ha Lee, Juan Carlos Gomora, Leanne L. Cribbs, and Edward Perez-Reyes
Department of Physiology, Loyola University Medical Center, Maywood, Illinois 60153 USA

ABSTRACT Nickel has been proposed to be a selective blocker of low-voltage-activated, T-type calcium channels. However, studies on cloned high-voltage-activated Ca^{2+} channels indicated that some subtypes, such as α1E, are also blocked by low micromolar concentrations of $NiCl_2$. There are considerable differences in the sensitivity to Ni^{2+} among native T-type currents, leading to the hypothesis that there may be more than one T-type channel. We confirmed part of this hypothesis by cloning three novel Ca^{2+} channels, α1G, H, and I, whose currents are nearly identical to the biophysical properties of native T-type channels. In this study we examined the nickel block of these cloned T-type channels expressed in both *Xenopus* oocytes and HEK-293 cells (10 mM Ba^{2+}). Only α1H currents were sensitive to low micromolar concentrations (IC_{50} = 13 μM). Much higher concentrations were required to half-block α1I (216 μM) and α1G currents (250 μM). Nickel block varied with the test potential, with less block at potentials above −30 mV. Outward currents through the T channels were blocked even less. We show that depolarizations can unblock the channel and that this can occur in the absence of permeating ions. We conclude that Ni^{2+} is only a selective blocker of α1H currents and that the concentrations required to block α1G and α1I will also affect high-voltage-activated calcium currents.

INTRODUCTION

Classification of voltage-gated Ca^{2+} channels has relied on their distinctive biophysical and pharmacological properties. Biophysical criteria that distinguish T-type from other Ca^{2+} channel types include: 1) their activation at lower voltages (LVA), 2) inactivation at lower voltages, 3) their transient kinetics, 4) smaller single-channel conductance in isotonic $BaCl_2$, and 5) their slower deactivation (Carbone and Lux, 1984; Fox et al., 1987b; Matteson and Armstrong, 1986). Many studies have exploited their inactivation properties to isolate the T-type current, by subtracting the currents elicited during depolarizing pulses from a well-hyperpolarized potential (−90 mV) from those recorded from a more depolarized potential (−50 mV). In contrast to high-voltage-activated calcium channels, T channels do not have a distinctive pharmacology, because they are relatively resistant to most organic calcium channel blockers, such as the dihydropyridines that block L-type; peptide toxins, such as the snail toxin ω-conotoxin GVIA that blocks N-type; and the spider toxin ω-agatoxin-IVA that blocks P-type channels (reviewed in Miljanich and Ramachandran, 1995). Recently mibefradil has been suggested to be a selective blocker of T channels (Mishra and Hermsmeyer, 1994); however, it is only ~15-fold selective, and its block is highly sensitive to the holding potential (Bezprozvanny and Tsien, 1995; McDonough and Bean, 1998). Low concentrations of Ni^{2+} (<50 μM) have been used to selectively block T-type currents in a number of cell types, such as sinoatrial nodal cells (Hagiwara et al., 1988) and sensory neurons (Todorovic and Lingle, 1998). On the contrary, T-type currents in various neuronal cells require much higher doses of Ni^{2+} to be blocked (reviewed in Huguenard, 1996, and Todorovic and Lingle, 1998).

Molecular cloning of voltage-gated Ca^{2+} channels has revealed the existence of at least 10 genes (Lee et al., 1999a). One goal of these studies is to correlate the biophysical and pharmacological properties of the cloned channels with their native counterparts. Largely based on its nickel sensitivity and inactivation at negative holding potentials, a rat α1E was proposed to encode a member of the low-voltage-activated family (Soong et al., 1993). Subsequent studies with mouse, rabbit, and human clones concluded that α1E encoded a high-voltage-activated channel, the native counterparts of which are called R-type (Wakamori et al., 1994; Williams et al., 1994; Randall and Tsien, 1997; Zhang et al., 1993). One complication to these studies is that auxiliary subunits can alter the voltage-dependent gating of HVA α1 subunits, and the subunit structure of native R-type channels is not known. Notably, a novel $\alpha 2\delta$ isoform ($\alpha 2\delta$-2) was shown to shift the gating of α1E currents to lower potentials (Klugbauer et al., 1999). Therefore it is possible that α1E can generate low-threshold currents, as suggested by antisense oligonucleotide studies (Piedras-Renteria et al., 1997).

Recently our laboratory cloned three distinct α1 subunits of T-type calcium channels (Perez-Reyes et al., 1998a; Cribbs et al., 1998; Lee et al., 1999b). Expression of these cloned channels in either *Xenopus* oocytes or HEK-293 cells led to the induction of classical T-type currents in terms of their activation at low voltages, slow deactivation, and small conductance in isotonic $BaCl_2$. The goals of the present study were to determine the Ni^{2+} sensitivities of these three T-type channels and to investigate the mecha-

Received for publication 4 June 1999 and in final form 12 August 1999.

Address reprint requests to Dr. Edward Perez-Reyes, Department of Pharmacology, University of Virginia, 1300 Jefferson Park Avenue, Charlottesville, VA 22908. Tel.: 804-982-4440; Fax: 804-982-3878; E-mail: eperez@virginia.edu.

0006-3495/99/12/3034/09 $2.00

nisms of block. Our hypothesis was that the large discrepancies reported for the Ni^{2+} block of native T currents may be due to inherent differences in the sensitivities of the three subtypes. In contrast to the widespread belief that T currents are Ni^{2+} sensitive, we find that α1G and α1I are relatively insensitive to Ni^{2+}. Only α1H is blocked by low micromolar concentrations of $NiCl_2$. These observations, coupled with their distribution (Talley et al., 1999), provide an explanation for the reports of Ni^{2+}-insensitive T-type channels.

MATERIALS AND METHODS

Materials

Cloning of the full-length rat α1G cDNA was reported previously (Perez-Reyes et al., 1998a), as was its subcloning into pGEM-HEA (Chuang et al., 1998). This vector contains 5′ and 3′ untranslated regions from a *Xenopus* β globin gene, resulting in high levels of expression (Liman et al., 1992). The full-length human α1H cDNA (Cribbs et al., 1998) was also subcloned into pGEM-HEA. Cloning of the rat α1I cDNA and its subcloning into pSP73 along with 5′ globin sequences (Promega, Madison, WI) were described previously (Lee et al., 1999b). Generation of stably transfected HEK cell lines was described by Lee et al. (1999). All cell culture reagents were from Life Technologies (Grand Island, NY). Nickel(II) chloride hexahydrate ($NiCl_2$) was obtained from Aldrich (no. 20, 386-6; Milwaukee, WI). All other reagents were from Sigma (St. Louis, MO).

Electrophysiological analysis of injected oocytes

Capped cRNA was synthesized from plasmid linearized using T7 RNA polymerase (Ambion, Austin, TX). The concentration of cRNA was measured spectrophotometrically. Oocytes were prepared from *Xenopus laevis* (Xenopus One, Ann Arbor, MI) by standard techniques (Leonard and Snutch, 1991). Each oocyte was injected with 2–10 ng of cRNA in a volume of 50 nl.

Oocytes were voltage-clamped using a two-microelectrode voltage clamp amplifier (OC-725B; Warner Instrument Corp., Hampden, CT). The standard bath solution contained the following: 10 mM $Ba(OH)_2$, 90 mM NaOH, 1 mM KOH, and 5 mM HEPES, adjusted to pH 7.4 with methanesulfonic acid. Voltage and current electrodes (0.5–1.5 MΩ tip resistance) contained an agarose cushion and were filled with 3 M KCl (Schreibmayer et al., 1994). Data were acquired at 5 kHz with the pCLAMP system (Digidata 1200 and pCLAMP 6.0; Axon Instruments, Foster City, CA) and filtered at 1 kHz (no. 902 filter; Frequency Devices, Haverhill, MA).

Electrophysiological analysis of HEK-293-transfected cells

HEK-293 cells were dissociated by digestion with 0.25% trypsin plus 1 mM EDTA (Life Technologies) for 2 min, then diluted 20-fold with Dulbecco's minimum essential medium. The cells were triturated, diluted twofold with Dulbecco's minimum essential medium, and then plated on coverslips. The cells were incubated for at least 4 h and for up to 2 days before electrophysiological studies. The recording solution contained the following (in mM): 10 $BaCl_2$, 140 tetraethylammonium (TEA) chloride, 6 CsCl, and 10 HEPES (pH adjusted to 7.4 with TEA-OH). The standard internal pipette solution contained the following (in mM): 55 CsCl, 75 $CsMeSO_4$, 10 $MgCl_2$, 0.1 EGTA, and 10 HEPES (pH adjusted to 7.2 with CsOH). As noted, some experiments were performed with the following internal solution (in mM): 120 *N*-methyl-D-glucamine (NMDG), 10 EGTA, and 10 HEPES (pH adjusted to 7.2 with methanesulfonic acid).

Whole-cell currents were recorded from ruptured patches, using an Axopatch 200A amplifier, Digidata 1200 A/D converter, and pCLAMP 6.0 software (Axon Instruments). Data were digitized at 4 kHz and filtered at 1 kHz. Pipettes were made from TW-150-6 capillary tubing (World Precision Instruments, Sarasota, FL), using a model P-97 Flaming-Brown pipette puller (Sutter Instrument Co., Novato, CA). Under these solution conditions the pipette resistance was typically 1.5–2.0 MΩ. Series resistance (correction and prediction) and cell capacitance were compensated by at least 80%. The average cell capacitance was ~25 pF. All experiments were performed at room temperature.

Dose-response analysis

A 100 mM $NiCl_2$ stock solution was used for dilutions in deionized water, which were then diluted by at least 1:100 with the appropriate bath solution. The stock was stored at room temperature. Dilutions were made on the day of the experiment. The recording chamber for both oocyte and HEK-293 experiments was a RC-25 (Warner Instrument Corp.), which has a volume of 0.15 ml. Each test solution was either perfused at 2–4 ml/min, or 2 ml was slowly added directly to a static bath. Similar results were obtained with the two methods. Experiments designed to test reversibility used continuous perfusion. Leak currents were minimal at −30 mV in both oocytes and HEK-293 cells; therefore online leak subtraction was only used during measurement of the current-voltage (*I-V*) relationship (P/-6 or P/-4) or during the unblock experiments. Rundown and time-dependent shifts in the gating were observed in HEK-293 cells, especially for α1H; therefore we performed these experiments with oocytes. Experiments were only performed on cells in which the initial rate of rundown was less than 1% over the first 2 min of recording.

Data analysis

Peak currents and exponential fits to currents were determined using Clampfit software (Axon Instruments). Dose-response analysis and graphing of the data were done with Prism (GraphPad, San Diego, CA). Average data are presented as mean ± SEM.

RESULTS

Injection of cRNAs derived from cloned T-type calcium channel α1 subunits, α1G, α1H, and α1I, induced robust expression of T-type currents in *Xenopus* oocytes. The amount of cRNA injected was titrated so that the currents, using 10 mM Ba^{2+} as the charge carrier, were ~1 μA. At this level of expression, the possible contribution of endogenous currents would be less than 1% (Lacerda et al., 1994). To determine the dose dependence of Ni^{2+} block, several concentrations of $NiCl_2$ solutions were applied sequentially, and their effects were measured every 15 s by a test pulse of −30 mV from a holding potential of −90 mV. A typical experiment using oocytes injected with α1H is shown in Fig. 1, with representative current traces shown in the inset. $NiCl_2$ block was fast and reversible. $NiCl_2$ also slowed the inactivation kinetics, with little change in activation kinetics (Fig. 1 *B*). Because we have observed significant differences in the biophysical properties of α1I depending on the expression system (Lee et al., 1999b), we performed similar experiments using stably transfected HEK-293 cells. The currents from these stable cell lines are typically greater than 1 nA (Lee et al., 1999b), so there should be little contribution from endogenous currents (Berjukow et al.,

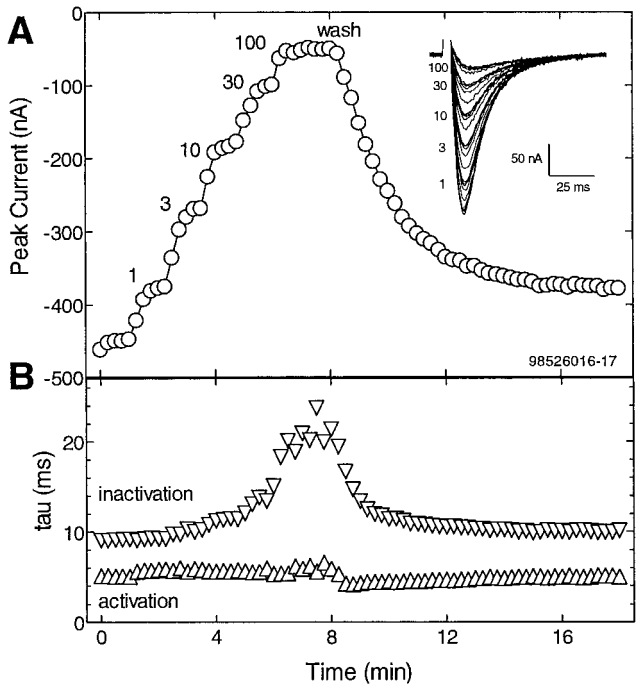

FIGURE 1 Nickel block of α1H currents expressed in *Xenopus* oocytes. Typical responses to increasing concentrations of $NiCl_2$, followed by washout. Test pulses to −30 mV from a holding potential of −90 mV were delivered every 15 s. The peak current was calculated and then plotted against time. Approximate times when $NiCl_2$ containing bath solutions were added are indicated (μM). *Inset*: Traces recorded from the same experiment. The current traces were simultaneously fit with two exponentials, with one phase representing activation kinetics (△) and the other inactivation (▽).

1996). Endogenous HEK-293 currents were not observed under our experimental conditions.

Cumulative dose-response analysis was performed on α1G, H, and I, expressed in both oocytes and HEK-293 cells (Fig. 2). Only α1H was significantly blocked by low micromolar concentrations of $NiCl_2$. The concentration at which half the α1H current was blocked (IC_{50}) was 6 μM in oocytes and 13 μM in HEK-293 cells. In contrast, the IC_{50} values determined for α1I were 15-fold higher, and ~24-fold higher for α1G currents (Table 1). The Hill slopes for the α1G and α1I curves were close to 1 in both systems, while the curves for α1H had slopes around 0.7 (Table 1). Channels expressed in oocytes were more sensitive to Ni^{2+} block than in HEK-293 cells, with α1I showing the largest difference (2.5-fold).

We next examined the voltage dependence of Ni^{2+} block of channels expressed in oocytes. Fig. 3 shows results obtained from oocytes injected with α1G. Representative traces taken during an *I-V* protocol under control conditions and in the presence of 300 μM $NiCl_2$ are shown in Fig. 3, *A* and *B*, respectively. The peak currents were averaged and plotted as a function of the test potential (Fig. 3 *C*). The data were obtained from three oocytes under control conditions and in the presence of 100, 300, and 1000 μM ($n = 2$) $NiCl_2$. In addition to blocking the current, Ni^{2+} appeared to

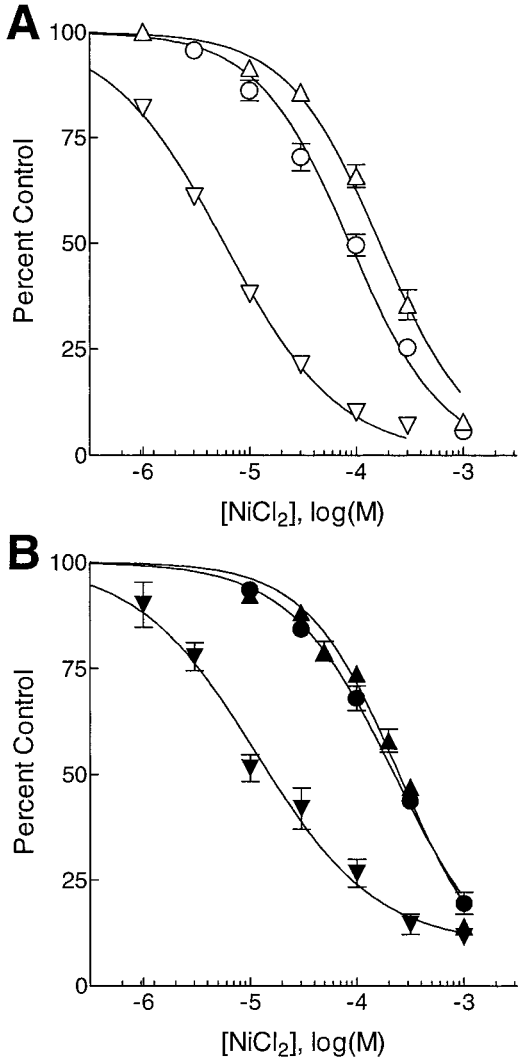

FIGURE 2 Dose-response analysis of Ni^{2+} block of α1G, H, and I currents. Responses were recorded from cloned channels expressed in either (*A*) oocytes or (*B*) HEK-293 cells. Data represent the average responses from four to seven cells (α1G, △, ▲; α1H, ▽, ▼; α1I, ○, ●). Smooth curves represent the fit to the data. In contrast to α1G and I, Hill coefficients for the α1H curves were significantly less than unity (Table 1).

shift the *I-V* curves to more depolarized potentials. This shift can be seen when the currents are normalized to the maximum current observed during the *I-V* protocol (Fig. 3 *D*). To quantitate this shift we calculated the chord conductance (Fig. 3 *E*) and normalized it to the maximum (Fig. 3

TABLE 1 Summary of the dose-dependent block by $NiCl_2$ deduced from test pulses to −30 mV

	Oocytes		HEK-293 cells	
	IC_{50} (μM)	Hill slope	IC_{50} (μM)	Hill slope
α1G	167 ± 15	−1.12 ± 0.11	250 ± 22	−1.00 ± 0.10
α1H	5.7 ± 0.3	−0.78 ± 0.04*	12 ± 2	−0.77 ± 0.09*
α1I	87 ± 7	−0.90 ± 0.06	216 ± 9	−0.89 ± 0.03*

*Significantly less than 1.

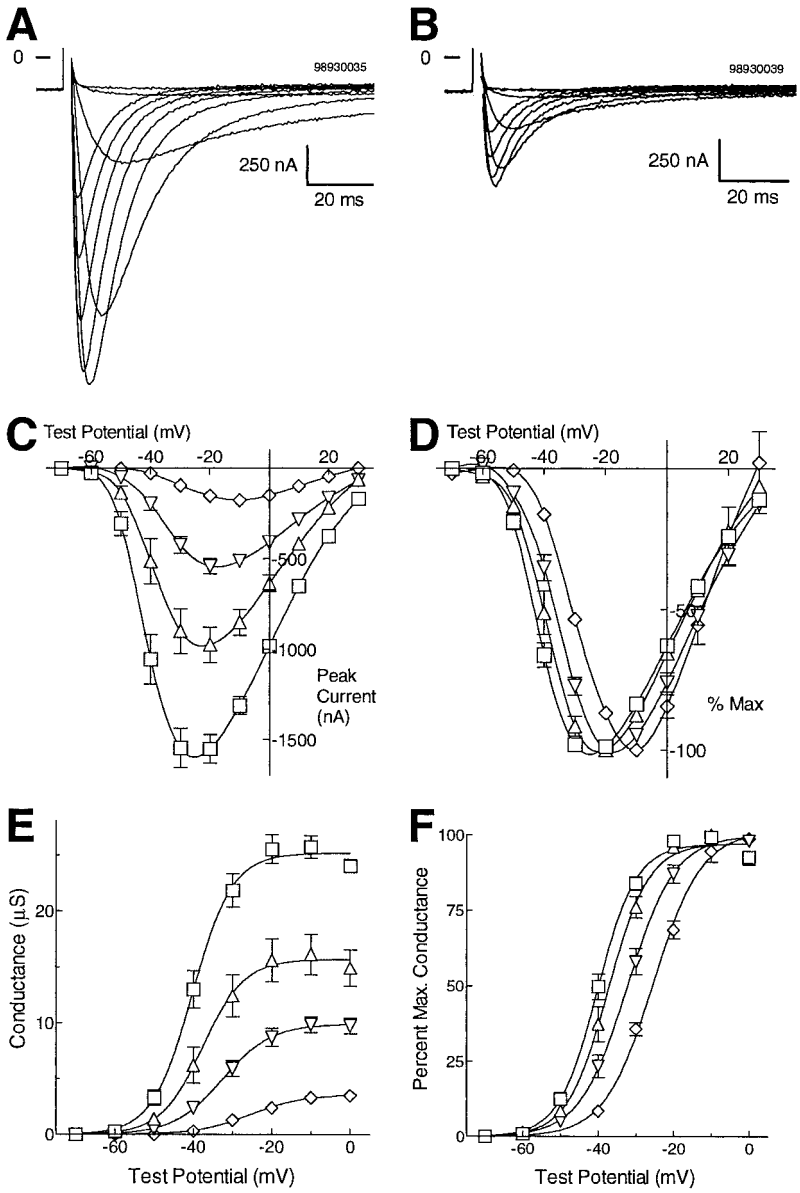

FIGURE 3 Voltage dependence of Ni^{2+} block. Data were recorded from oocytes injected with α1G. Currents were obtained during an *I-V* protocol in the absence (*A*) and presence (*B*) of 300 μM $NiCl_2$. For display purposes, the data were decimated by a factor of 4, using pClamp software. (*C*) Average peak currents from three oocytes recorded for control (□) and in the presence of 0.1 (△), 0.3 (▽), and 1 mM $NiCl_2$ (◇). (*D*) The data in *C* were normalized to the maximum peak current observed in each cell and then averaged. (*E*) Conductance was calculated by dividing the observed current by the driving force (reversal potential minus the test potential) and then averaged. A constant reversal potential of 40 mV was used for all data sets. Measurement of the reversal potential in oocytes is complicated by small outward currents. The data in *E* were normalized to the maximum conductance observed during each *I-V* protocol and then averaged. Smooth curves in *E* and *F* are fits to the data calculated with the Boltzmann equation.

F). Boltzmann fits to the data were used to calculated the voltage at which half the channels open ($V_{0.5}$). The curve obtained in the presence of 1000 μM $NiCl_2$ was shifted 15 mV relative to control. Similar shifts were deduced when conductance was calculated using the Goldman-Hodgkin-Katz equation (Hille, 1992). Similar results were obtained with cloned HVA α1 subunits (Zamponi et al., 1996) and were interpreted as Ni^{2+} binding to two sites: one that blocks conductance and a second site that alters channel gating. An alternative explanation is that block is simply voltage dependent.

To illustrate the voltage dependence of block we plotted the percentage block of the peak current as a function of the test potential (Fig. 4 *A*). $NiCl_2$ concentrations were chosen that were slightly above the IC_{50} value for each channel (α1H, 10 μM; α1G and I, 300 μM). Block of α1G and α1I was greatest during test pulses to −50 mV and decreased 20% to a plateau at 0 mV (Fig. 4 *A*). In contrast, block of α1H was essentially voltage independent over the potentials tested (Fig. 4 *B*). A consequence of this voltage dependence is that the apparent sensitivity of the channel will depend on the test potential used (Fig. 4 *C*). The apparent IC_{50} of α1G currents decreased from 200 μM at 0 mV to 70 μM at −40 mV. Similar results were obtained with α1I (data not shown). In contrast, the apparent sensitivity of α1H channels did not depend on the test potential (Fig. 4 *B*).

From the analysis shown in Fig. 3, *E* and *F*, we plotted the dose dependence of nickel's block of the maximum conductance and its apparent shift in gating and then fit the data with the dose-response equation. The IC_{50} values calculated from the maximum conductance were similar to the values obtained from a single pulse to −30 mV (Table 1): α1G, 169 ± 10 μM; α1H, 6 ± 2 μM; and α1I, 168 ± 2 μM. Plots of the shift in $V_{0.5}$ versus $NiCl_2$ concentration did

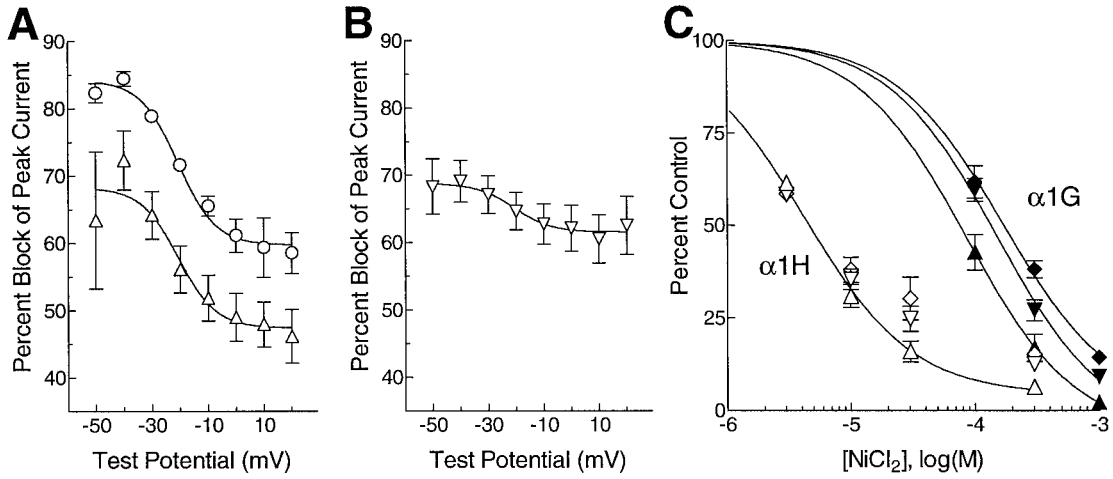

FIGURE 4 Nickel block is voltage dependent. (*A* and *B*) The percentage block by $NiCl_2$ was calculated for each potential. Conductance was calculated from *I-V* protocols as described in Fig. 3. The data were obtained from oocytes expressing either α1G (△, $n = 3$, 300 μM $NiCl_2$), α1H (▽, $n = 6$, 10 μM $NiCl_2$), or α1I (○, $n = 3$, 300 μM $NiCl_2$). Smooth curves represent Boltzmann fits ($V_{50} = -21$ mV, $k = -7$, for α1G, H, and I). (*C*) The dose response of α1G (▲, ▼, ◆) and α1H (△, ▽, ◇) to $NiCl_2$ was calculated from data obtained during test pulses to −40 (△, ▲), −20 (▽, ▼), and 0 mV (◇, ◆). Smooth curves represent fits to the data, assuming a Hill coefficient of 1.

not reach saturation at the doses tested (up to 1 mM); therefore this IC_{50} can only be estimated: α1G, 682 ± 47 μM; α1H, 35 ± 9 μM; and α1I, 454 ± 100 μM. For all three channels the IC_{50} for block of the maximum conductance was lower than the shift in gating. This difference was largest for α1H (sixfold). The ability of Ni^{2+} to shift the $V_{0.5}$ was similar for α1G and I channels. In contrast, the shift in α1H gating occurred at lower concentrations.

If Ni^{2+} is blocking inward current by binding in the pore, then we reasoned that outward currents may knock it off, as observed previously for charybdotoxin block of Ca^{2+}-activated K^+ channels (MacKinnon and Miller, 1988). Expression of cloned T channels in oocytes and HEK-293 cells leads to the appearance of outward currents during test potentials above +40 mV. These currents decay with the same kinetics as the inward current (Fig. 5, *A* and *B*). It is likely that these currents are carried by K^+, because oocytes contain 150 mM K^+ (Dascal et al., 1986). For both α1G and α1I, 300 μM Ni^{2+} produced over 50% block of the inward current, with little block of the outward current. This effect was most pronounced for α1I: block approaches a voltage-independent value of 60% at −10 mV (Fig. 4 *A*) and continues up to +20 mV, then abruptly disappears at test potentials beyond the reversal potential (Fig. 5 *F*; +60 mV, 3%). In contrast, there is still significant block of the outward current carried by α1G (+60 mV, 72%). Another difference between α1G and α1I was the apparent reversal potential, which was 10 mV more positive for α1G. These differences suggest that T channel subtypes may differ in their permeability properties, and this may account for the difference in nickel's ability to block the outward current. For example, the pore of α1G may bind Ba^{2+} and Ni^{2+} more tightly, thereby reducing outward currents in control and leading to less Ni^{2+} block of the outward currents.

An alternative hypothesis for explaining the unblock is that large depolarizations induce changes in channel structure, leading to a conformation with lower affinity for Ni^{2+}. Although such changes in T-type channel gating have not been reported, large depolarizations have been reported to affect L-type gating, driving the channels into a high activity mode (Pietrobon and Hess, 1990). In this case, unblock would occur even in the absence of permeant ions, as observed for the unblock of P-type channels by ω-agatoxin IVA (McDonough et al., 1997). To gain control of the intracellular milieu, we switched to the ruptured-patch clamp of α1I-transfected HEK-293 cells. Experiments using Cs^+-based intracellular solutions and cells stably transfected with α1I yielded results similar to those observed in oocytes (Fig. 6, *A* and *B*), that is, outward currents during test depolarizations above +40 mV that had kinetics similar to those of the inward currents, and little or no block of these outward currents, even at concentrations that blocked more than half of the inward current. To induce unblock, we inserted a step depolarization during a −30-mV step, then varied its potential in 20-mV steps (Fig. 6 *A, inset*). We used a −30-mV step because we measured maximum block at this potential (Fig. 4 *A*). Further depolarization during the prepulse led to an increase in the amplitude of the tail current that decayed monoexponentially under control conditions (Fig. 6 *C*). One explanation is that not all channels are activated at −30 mV, so that further depolarization activates more channels, producing a larger tail current. An alternative explanation is that there is a blocking ion in control solutions. In the presence of 300 μM Ni^{2+} (Fig. 6 *B*), the tail currents after the depolarization approached the amplitude observed in control, then decayed biexponentially. These results suggest that the large depolarization had

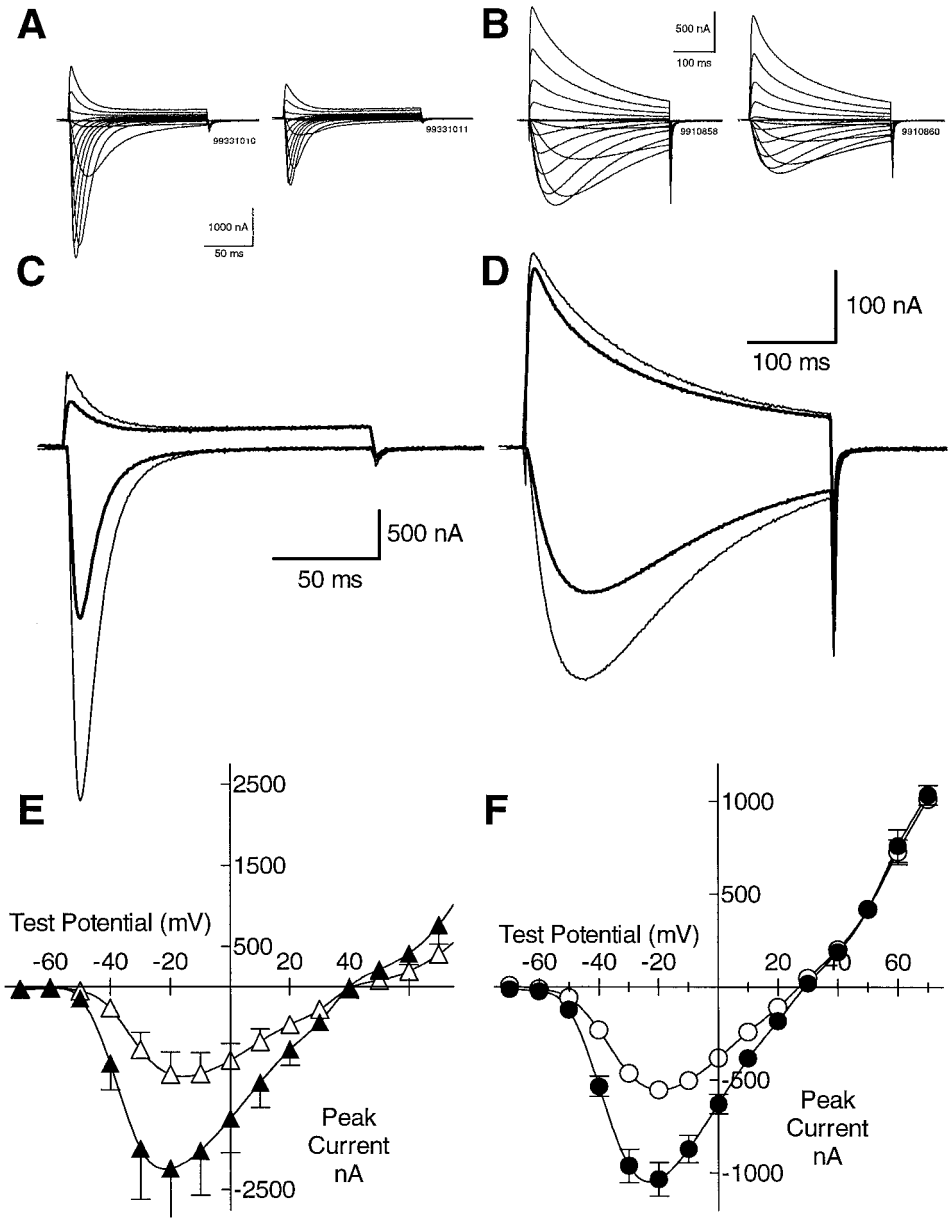

FIGURE 5 Nickel does not block outward currents. Representative traces obtained during an *I-V* protocol are shown for control and in the presence of 300 μM $NiCl_2$. (*A*) Currents recorded from α1G-injected oocytes under control conditions (*left*) and in the presence of $NiCl_2$ (*right*). (*B*) Currents recorded from α1I-injected oocytes under control conditions (*left*) and in the presence of $NiCl_2$ (*right*). (*C, D*) data from *A* and *B*, respectively, for test depolarizations to -20 and $+60$ mV in the absence and presence of $NiCl_2$ (*dark lines*) are superimposed. Average results for α1G are plotted in *E*, and those obtained for α1I are shown in *F*.

caused unblock of the channel, and that upon repolarization the channels were rapidly reblocked, as observed previously for Cd^{2+} block of high-voltage-activated Ca^{2+} channels (Thevenod and Jones, 1992). By fixing the first exponential to that observed in control (31 ms), we calculated a second exponential of 2.7 ± 0.5 ms ($n = 3$), which at this concentration would correspond to a bimolecular association constant of $3.7 \times 10^6\ M^{-1}\ s^{-1}$. The unblock of channels during a pulse might explain why Ni^{2+} slows inactivation kinetics (Fig. 1 *B*).

Surprisingly, we also observed unblock in experiments in which the intracellular solution contained *N*-methyl-D-glucamine (NMDG) instead of Cs^+ (Fig. 6, *D* and *E*). No outward currents were detected even at $+110$ mV, indicating that NMDG does not permeate α1I channels. As observed with intracellular Cs^+ solutions, the tail currents in the presence of Ni^{2+} decayed biexponentially. We calculated the fractional unblock using the equation

$$\text{Fractional unblock} = (\text{maximal block} - \text{residual block})/\text{maximal block}$$

where the maximum block was the block observed during the -30-mV pulse, and the residual block was the block observed at the peak of the tail current. Unblock was apparent after depolarizations to -10 mV and approached a maximum after $+110$-mV steps. Fractional unblock after $+110$-mV depolarizations was greater in Cs^+-containing solutions than in those containing NMDG (Fig. 6 *F*). These results indicate that two mechanisms are responsible for unblock, one that is voltage dependent, and a second that involves outward monovalent cation flux.

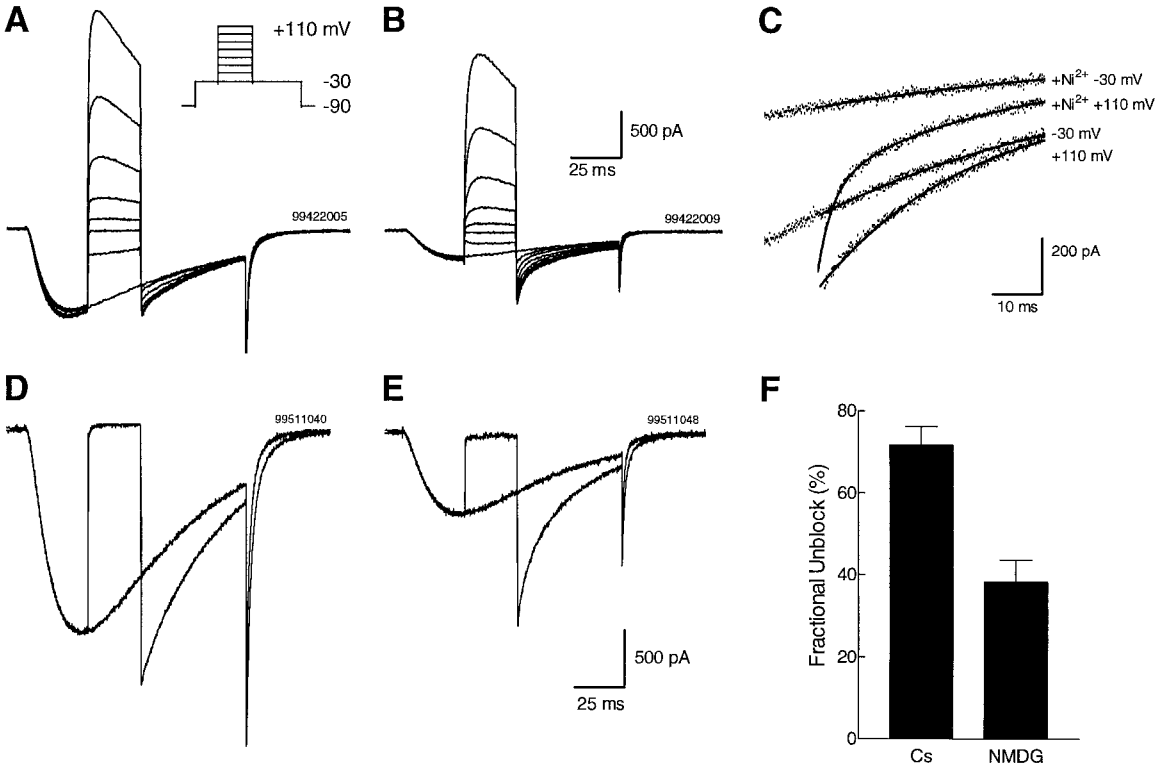

FIGURE 6 Relief of nickel block at extreme positive voltages. Representative traces were obtained from α1I-transfected HEK-293 cells, using Cs^+ as the main intracellular cation in the absence (*A*) and in the presence (*B*) of 300 μM $NiCl_2$ in the bath solution (2 mM $BaCl_2$, 140 TEA-Cl, 6 CsCl, and 10 HEPES, pH adjusted to 7.4 with TEA-OH). (*C*) Reblock of Ca^{2+} channels by Ni^{2+} at -30 mV after unblocking by depolarization to $+110$ mV. Tail currents generated by repolarization to -30 mV were fit (*solid lines*) with one (control) or two ($+$ Ni^{2+}) exponentials. The same data are shown in *A* and *B*. (*D, E*) Current traces obtained using the same protocol, but using NMDG as the main cation in the pipette solution. Traces were obtained from the same cell in the absence (*D*) and in the presence (*E*) of 300 μM $NiCl_2$. Although with NMDG outward currents were not produced, some unblock still occurred. (*F*) Percentage of fractional unblock induced by a depolarization to $+110$ mV with Cs or NMDG. The initial amplitude of the exponential fits (as shown in *C*) was used to calculate the fractional unblock. Results represent the mean $\pm$ SEM ($n = 3$ for each cation).

DISCUSSION

The major finding of the present study is that of the three cloned T channels, only α1H is blocked by low micromolar concentrations of Ni^{2+}. We also studied the biophysical properties of Ni^{2+} block and showed that these properties are similar to those observed previously for HVA channels. These similarities exist despite the low level of sequence conservation, indicating considerable structural conservation. We present evidence that Ni^{2+} blocks less during positive test potentials. As a consequence, Ni^{2+} appears to be affecting channel gating (Zamponi et al., 1996). We also show that Ni^{2+} blocks the outward current much less than the inward current. Unblock of the channel at positive potentials can occur in the absence of permeating ions. Similar results were obtained with block of HVA channels by Cd^{2+} (Thevenod and Jones, 1992) and by ω-agatoxin IVA (McDonough et al., 1997).

The notion that T-type channels were selectively blocked by low concentrations of Ni^{2+} began with the classic studies of Hagiwara et al. (1988). Using rabbit sinoatrial nodal cells, they showed that 40 μM $NiCl_2$ selectively blocked the transient, low-voltage-activated Ca^{2+} current (T-type), with little effect on the long-lasting, dihydropyridine-sensitive (L-type) current. They then went on to show that T-type channels contributed to the late phase of the pacemaker depolarization. Although detailed dose-response relationships have not been published, many studies of mammalian cardiac myocytes have reported complete block of the T current by 30–50 μM $NiCl_2$, with little or no effect on the L-type current (Zhou and Lipsius, 1994; Satoh, 1995). Based on the present results and the fact that we cloned α1H from a human heart cDNA library (Cribbs et al., 1998), we suggest that α1H is the predominant isoform expressed in heart. Similarly, sensory neurons of the dorsal root ganglia predominantly express α1H (Talley et al., 1999), and their T currents are completely blocked by 100 μM $NiCl_2$ (Fox et al., 1987a; Todorovic and Lingle, 1998). T currents in cardiac Purkinje fibers have been reported to be less sensitive to Ni^{2+}, with 50 μM producing 47% block and only 72% block at 500 μM (Tseng and Boyden, 1989), although Hirano et al. (1989) reported that 100 μM produced nearly complete block. Northern blot analysis indicates that heart also expresses mRNA for α1G (Perez-Reyes et al., 1998a), which we show encodes T channels that are relatively Ni^{2+}

insensitive. Therefore it is likely that Purkinje fibers express α1G channels. We plan to investigate this hypothesis further using immunolocalization.

Similar to T-type channels in pacemaker cells, relatively Ni^{2+}-sensitive T-type currents were reported from rat aorta smooth muscle cells (IC_{50} = 10 μM; Akaike et al., 1989), rat amygdala (IC_{50} = 30 μM; Kaneda and Akaike, 1989), and medullary thyroid carcinoma (TT) cells (IC_{50} = 5 μM; Mlinar and Enyeart, 1993). We suggest that these cells predominantly express α1H. In agreement with the present results obtained with α1H, Mlinar and Enyeart (1993) showed that Ni^{2+} block of the TT cell current was relatively voltage independent, and that its dose dependency had a Hill slope of −0.6. Additional support for this conclusion comes from the recent work of Williams et al. (1999), who cloned an α1H cDNA from a TT cell cDNA library, which is 99.2% identical to our α1H at the nucleotide level (Cribbs et al., 1998). Nickel was also a potent blocker (IC_{50} = 6.6 μM; 15 mM Ba^{2+} as charge carrier) of their cloned α1H expressed in HEK-293 cells.

The reported Ni^{2+} sensitivity of neuronal T channels is quite variable (Huguenard, 1996). One possible explanation for this variability is that each study used a different charge carrier at different concentrations, which may affect block. For example, studies used either Ca^{2+} or Ba^{2+} at concentrations ranging from 2 to 50 mM. However, many studies used 10 mM, so a comparison to the present results can be made. Our results indicate that there are two other explanations: 1) the apparent affinity will depend on the test voltage and 2) distinct isoforms have very different sensitivities. In situ hybridization studies indicated that α1G is the predominant isoform expressed in brain (Talley et al., 1999) and is expressed in the same regions where Ni^{2+}-insensitive T currents have been recorded, such as hippocampus (IC_{50} = 230 μM; Ye and Akaike, 1993), frontal cortex (IC_{50} = 260 μM; Takahashi and Akaike, 1991), and thalamus (83% block at 500 μM; Suzuki and Rogawski, 1989). In many brain regions α1G is coexpressed with α1I, as in cerebellum and the inferior olive, while hippocampus and olfactory bulb express all three isoforms. Based on their distribution, we conclude that Ni^{2+} block of the cloned T channels correlates well with the Ni^{2+} sensitivity of native T currents.

This conclusion is supported by our results that the biophysical properties of the cloned channels in HEK-293 cells are nearly identical to those reported for native T currents (Lee et al., 1999b). In contrast, the biophysical and pharmacological properties of cloned high-voltage-activated α1 subunits do not match native currents, and numerous studies have documented the important role of auxiliary subunits in determining these properties. Currents through α1I channels were more sensitively blocked by Ni^{2+} when expressed in *Xenopus* oocytes than those in HEK293 cells. A plausible interpretation for the difference is that HEK-293 cells express unidentified auxiliary subunits for T-type channels, which might alter Ni^{2+} sensitivity. The presence of auxiliary subunits for T-type channels was previously proposed from the kinetic differences of α1I currents between the two expression systems (Lee et al., 1999b). Regardless of the mechanism, α1I currents in oocytes activated and inactivated much more slowly, which would allow for more channels to be in the open state during a test depolarization. Because Ni^{2+} is in part an open-channel blocker, these slower kinetics may in part explain the differences in sensitivity.

Zamponi et al. (1996) performed a detailed study of the nickel block of the cloned HVA α1A, B, C, and E subunits (Zamponi et al., 1996). They concluded that Ni^{2+} had two actions: it blocked currents and it shifted the voltage dependence of gating. They also showed that β subunits dramatically altered nickel's ability to shift gating. Of these channels, the apparent gating of α1E was the most dramatically affected by Ni^{2+}, being shifted by over 30 mV. We have obtained similar results with human α1E (Lee and Perez-Reyes, unpublished observations). One difference between these studies is that we find block occurring at lower concentrations than the shift, while they had the opposite result. Despite the fact that T channels are only 15% identical to HVA α1 subunits at the amino acid level, the consequences of Ni^{2+} block are similar. This suggests that Ni^{2+} is binding to regions that are conserved between the channels. Two regions that are likely to be involved, the S4 and pore loops, are well conserved (Perez-Reyes et al., 1998b). These regions are more highly conserved between the members of a subfamily; for example, the four pore loops of α1H are 96% identical to α1G, making it difficult to deduce a Ni^{2+} binding site. A second difference between the studies is in the interpretation of the results; we suggest that the shift in gating is due in part to Ni^{2+} block of closed states followed by unblock of the open state at potentials higher than −30 mV. Clearly the effects of Ni^{2+} are complex, with more than one mechanism. At one extreme are channels like α1H that can be blocked with little effect on gating, while at the other extreme there are channels like α1E, where the apparent shift in gating occurs before substantial block of the peak current. In any case, combining the results of these two studies allows us to deduce the following rank order of nickel sensitivity: α1H $\gg$ α1C $>$ α1I $>$ α1G $>$ α1E $>$ α1A $\gg$ α1B. We conclude that α1H is the subunit that forms the most Ni^{2+}-sensitive Ca^{2+} channels.

We thank Qun Jiang for technical assistance. We thank Dr. Stephen W. Jones for helpful comments on a draft of this paper.

This work was supported in part by National Institutes of Health grants HL58728 and NS38691. EP-R is an Established Investigator of the American Heart Association.

REFERENCES

Akaike, N., H. Kanaide, T. Kuga, M. Nakamura, J. Sadoshima, and H. Tomoike. 1989. Low-voltage-activated calcium current in rat aorta smooth muscle cells in primary culture. *J. Physiol. (Lond.)*. 416: 141–160.

Berjukow, S., F. Doring, M. Froschmayr, M. Grabner, H. Glossmann, and S. Hering. 1996. Endogenous calcium channels in human embryonic kidney (HEK-293) cells. *Br. J. Pharmacol.* 118:748–754.

Bezprozvanny, I., and R. W. Tsien. 1995. Voltage-dependent blockade of diverse types of voltage-gated Ca^{2+} channels expressed in *Xenopus* oocytes by the Ca^{2+} channel antagonist mibefradil (Ro 40-5967). *Mol. Pharmacol.* 48:540–549.

Carbone, E., and H. D. Lux. 1984. A low voltage-activated, fully inactivating Ca channel in vertebrate sensory neurones. *Nature.* 310:501–502.

Chuang, R. S.-I., H. Jaffe, L. L. Cribbs, E. Perez-Reyes, and K. J. Swartz. 1998. Inhibition of T-type voltage-gated calcium channels by a new scorpion toxin. *Nature Neurosci.* 1:668–674.

Cribbs, L. L., J.-H. Lee, J. Yang, J. Satin, Y. Zhang, A. Daud, J. Barclay, M. P. Williamson, M. Fox, M. Rees, and E. Perez-Reyes. 1998. Cloning and characterization of α1H from human heart, a member of the T-type calcium channel gene family. *Circ. Res.* 83:103–109.

Dascal, N., T. P. Snutch, H. Lubbert, N. Davidson, and H. A. Lester. 1986. Expression and modulation of voltage-gated calcium channels after RNA injection in *Xenopus* oocytes. *Science.* 231:1147–1150.

Fox, A. P., M. C. Nowycky, and R. W. Tsien. 1987a. Kinetic and pharmacological properties distinguishing three types of calcium currents in chick sensory neurones. *J. Physiol. (Lond.).* 394:149–172.

Fox, A. P., M. C. Nowycky, and R. W. Tsien. 1987b. Single-channel recordings of three types of calcium channels in chick sensory neurones. *J. Physiol. (Lond.).* 394:173–200.

Hagiwara, N., H. Irisawa, and M. Kameyama. 1988. Contribution of two types of calcium currents to the pacemaker potentials of rabbit sino-atrial node cells. *J. Physiol. (Lond.).* 395:233–253.

Hille, B. 1992. Ionic Channels of Excitable Membranes. Sinauer Associates, Sunderland, MA.

Hirano, Y., H. A. Fozzard, and C. T. January. 1989. Characteristics of L- and T-type Ca^{2+} currents in canine cardiac purkinje cells. *Am. J. Physiol.* 256:H1478–H1492.

Huguenard, J. R. 1996. Low threshold calcium currents in central nervous system neurons. *Annu. Rev. Physiol.* 58:329–348.

Kaneda, M., and N. Akaike. 1989. The low-threshold Ca current in isolated amygdaloid neurons in the rat. *Brain Res.* 497:187–190.

Klugbauer, N., L. Lacinova, E. Marais, M. Hobom, and F. Hofmann. 1999. Molecular diversity of the calcium channel alpha2delta subunit. *J. Neurosci.* 19:684–691.

Lacerda, A. E., E. Perez-Reyes, X. Wei, A. Castellano, and A. M. Brown. 1994. T-type and N-type calcium channels of *Xenopus* oocytes: evidence for specific interactions with beta subunits. *Biophys. J.* 66:1833–1843.

Lee, J.-H., L. L. Cribbs, and E. Perez-Reyes. 1999a. Cloning of a putative four repeat ion channel from rat brain. *FEBS Lett.* 445:231–236.

Lee, J.-H., A. N. Daud, L. L. Cribbs, A. E. Lacerda, A. Pereverzev, U. Klockner, T. Schneider, and E. Perez-Reyes. 1999b. Cloning and expression of a novel member of the low voltage-activated T-type calcium channel family. *J. Neurosci.* 19:1912–1921.

Leonard, J. P., and T. P. Snutch. 1991. The Expression of Neurotransmitter Receptors and Ion Channels in *Xenopus* Oocytes. IRL Press, Oxford.

Liman, E. R., J. Tytgat, and P. Hess. 1992. Subunit stoichiometry of a mammalian K^+ channel determined by construction of multimeric cDNAs. *Neuron.* 9:861–871.

MacKinnon, R., and C. Miller. 1988. Mechanism of charybdotoxin block of the high-conductance, Ca^{2+}-activated K^+ channel. *J. Gen. Physiol.* 91:335–349.

Matteson, D. R., and C. M. Armstrong. 1986. Properties of two types of calcium channels in clonal pituitary cells. *J. Gen. Physiol.* 87:161–182.

McDonough, S. I., and B. P. Bean. 1998. Mibefradil inhibition of T-type calcium channels in cerebellar Purkinje neurons. *Mol. Pharmacol.* 54: 1080–1087.

McDonough, S. I., I. M. Mintz, and B. P. Bean. 1997. Alteration of P-type calcium channel gating by the spider toxin omega-Aga-IVA. *Biophys. J.* 72:2117–2128.

Miljanich, G. P., and J. Ramachandran. 1995. Antagonists of neuronal calcium channels: structure, function, and therapeutic implications. *Annu. Rev. Pharmacol. Toxicol.* 35:707–734.

Mishra, S. K., and K. Hermsmeyer. 1994. Selective inhibition of T-type Ca^{2+} channels by Ro 40-5967. *Circ. Res.* 75:144–148.

Mlinar, B., and J. J. Enyeart. 1993. Block of current through T-type calcium channels by trivalent metal cations and nickel in neural rat and human cells. *J. Physiol. (Lond.).* 469:639–652.

Perez-Reyes, E., L. L. Cribbs, A. Daud, A. E. Lacerda, J. Barclay, M. P. Williamson, M. Fox, M. Rees, and J.-H. Lee. 1998a. Molecular characterization of a neuronal low voltage-activated T-type calcium channel. *Nature.* 391:896–900.

Perez-Reyes, E., L. L. Cribbs, A. Daud, J. Yang, A. E. Lacerda, J. Barclay, M. P. Williamson, M. Fox, M. Rees, and J.-H. Lee. 1998b. Molecular characterization of T-type calcium channels. *In* Low Voltage-Activated T-Type Calcium Channels. R. W. Tsien, J.-P. Clozel, and J. Nargeot, editors. Adis International, Chester, UK. 290–305.

Piedras-Renteria, E. S., C. C. Chen, and P. M. Best. 1997. Antisense oligonucleotides against rat brain alpha1E DNA and its atrial homologue decrease T-type calcium current in atrial myocytes. *Proc. Natl. Acad. Sci. USA.* 94:14936–14941.

Pietrobon, D., and P. Hess. 1990. Novel mechanism of voltage-dependent gating in L-type calcium channels. *Nature.* 346:651–655.

Randall, A. D., and R. W. Tsien. 1997. Contrasting biophysical and pharmacological properties of T-type and R-type calcium channels. *Neuropharmacology.* 36:879–893.

Satoh, H. 1995. Role of T-type Ca^{2+} channel inhibitors in the pacemaker depolarization in rabbit sino-atrial nodal cells. *Gen. Pharmacol.* 26: 581–587.

Schreibmayer, W., H. A. Lester, and N. Dascal. 1994. Voltage clamping of *Xenopus laevis* oocytes utilizing agarose-cushion electrodes. *Pflugers Arch.* 426:453–458.

Soong, T. W., A. Stea, C. D. Hodson, S. J. Dubel, S. R. Vincent, and T. P. Snutch. 1993. Structure and functional expression of a member of the low voltage-activated calcium channel family. *Science.* 260:1133–1136.

Suzuki, S., and M. A. Rogawski. 1989. T-type calcium channels mediate the transition between tonic and phasic firing in thalamic neurons. *Proc. Natl. Acad. Sci. USA.* 86:7228–7232.

Takahashi, K., and N. Akaike. 1991. Calcium antagonist effects on low-threshold (T-type) calcium current in rat isolated hippocampal CA1 pyramidal neurons. *J. Pharmacol. Exp. Ther.* 256:169–175.

Talley, E. M., L. L. Cribbs, J.-H. Lee, A. Daud, E. Perez-Reyes, and D. Bayliss. 1999. Differential distribution of three members of a gene family encoding low voltage-activated (T-type) calcium channels. *J. Neurosci.* 19:1895–1911.

Thevenod, F., and S. W. Jones. 1992. Cadmium block of calcium current in frog sympathetic neurons. *Biophys. J.* 63:162–168.

Todorovic, S. M., and C. J. Lingle. 1998. Pharmacological properties of T-type Ca^{2+} current in adult rat sensory neurons: effects of anticonvulsant and anesthetic agents. *J. Neurophysiol.* 79:240–252.

Tseng, G.-N., and P. A. Boyden. 1989. Multiple types of Ca^{2+} currents in single canine Purkinje cells. *Circ. Res.* 65:1735–1750.

Wakamori, M., T. Niidome, D. Furutama, T. Furuichi, K. Mikoshiba, Y. Fujita, I. Tanaka, K. Katayama, A. Yatani, A. Schwartz, and Y. Mori. 1994. Distinctive functional properties of the neuronal BII (class E) calcium channel. *Receptors Channels.* 2:303–314.

Williams, M. E., L. M. Marubio, C. R. Deal, M. Hans, P. F. Brust, L. H. Philipson, R. J. Miller, E. C. Johnson, M. M. Harpold, and S. B. Ellis. 1994. Structure and functional characterization of neuronal alpha 1E calcium channel subtypes. *J. Biol. Chem.* 269:22347–22357.

Williams, M. E., M. S. Washburn, M. Hans, A. Urrutia, P. F. Brust, P. Prodanovich, M. M. Harpold, and K. A. Standerman. 1999. Structure and functional characterization of a novel human low-voltage activated calcium channel. *J. Neurochem.* 72:791–799.

Ye, J. H., and N. Akaike. 1993. Calcium currents in pyramidal neurons acutely dissociated from the rat frontal cortex: a study by the nystatin perforated patch technique. *Brain Res.* 606:111–117.

Zamponi, G. W., E. Bourinet, and T. P. Snutch. 1996. Nickel block of a family of neuronal calcium channels: subtype- and subunit-dependent action at multiple sites. *J. Membr. Biol.* 151:77–90.

Zhang, J. F., A. D. Randall, P. T. Ellinor, W. A. Horne, W. A. Sather, T. Tanabe, T. L. Schwarz, and R. W. Tsien. 1993. Distinctive pharmacology and kinetics of cloned neuronal Ca^{2+} channels and their possible counterparts in mammalian CNS neurons. *Neuropharmacology.* 32: 1075–1088.

Zhou, Z., and S. L. Lipsius. 1994. T-type calcium current in latent pacemaker cells isolated from cat right atrium. *J. Mol. Cell. Cardiol.* 26: 1211–1219.